Materials and Design 197 (2021) 109212

Contents lists available at ScienceDirect

Materials and Design

journal homepage: www.elsevier.com/locate/matdes

3D integration of pH-cleavable drug-hydrogel conjugates on magnetically driven smart microtransporters

Roberto Bernasconi [a,1], Emanuele Mauri [a,b,1], Arianna Rossetti [a], Stefano Rimondo [a], Raffaella Suriano [c], Marinella Levi [c], Alessandro Sacchetti [a], Salvador Pané [d], Luca Magagnin [a], Filippo Rossi [a,*]

[a] Department of Chemistry, Materials and Chemical Engineering "Giulio Natta", Politecnico di Milano, via Mancinelli 7, 20131 Milano, Italy
[b] Department of Engineering, Università Campus Bio-Medico di Roma, via Álvaro del Portillo 21, 00128 Rome, Italy
[c] Department of Chemistry, Materials and Chemical Engineering "Giulio Natta", Politecnico di Milano, piazza Leonardo da Vinci 32, 20133 Milano, Italy
[d] Multi-Scale Robotics Laboratory, Institute of Robotics and Intelligent Systems, ETH Zurich, Tannenstrasse 3, 8092 Zurich, Switzerland

HIGHLIGHTS

- Functionalized alginate hydrogels for pH controlled drug release are synthesized.
- Functionalization is designed to allow sustained drug release only at pH lower than 4.5.
- Hydrogels are applied on magnetically steerable devices able to navigate human body.
- Hydrogel coating onto microrobots create drug carriers that can reach specific target sites.
- Hydrogel coating functionalization can guarantee the release of drugs only in the target site.

GRAPHICAL ABSTRACT

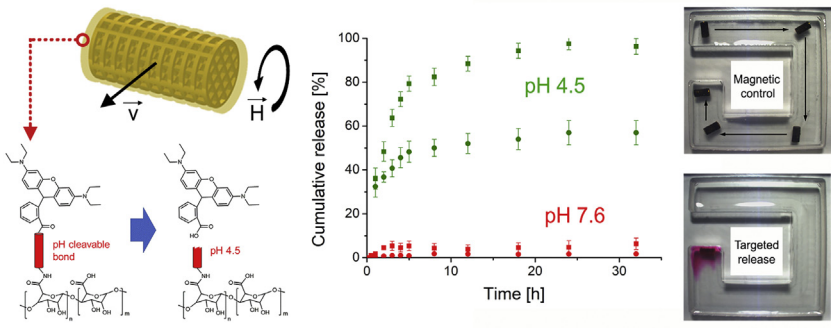

ARTICLE INFO

Article history:
Received 6 July 2020
Received in revised form 3 October 2020
Accepted 5 October 2020
Available online 08 October 2020

Keywords:
Drug delivery
pH cleavable
Hydrogel
Microdevices

ABSTRACT

Targeted drug delivery is currently emerging as a promising approach to overcome the limits of currently employed administration techniques. The most convenient methodology to control drug delivery is the application of stimuli-responsive materials, which can release drugs only when required, to remotely controlled microdevices able to navigate human body. Thanks to this synergy, release can be controlled both spatially and temporally. Spatial control is guaranteed by the maneuverability of the devices, which can be precisely guided to release in targeted locations. Temporal control, conversely, is guaranteed by the functionalization introduced in the stimuli-responsive material. In this context, the present work describes the coating of magnetically controlled microdevices with functionalized alginate-based hydrogels able to release drugs at pH values lower than 4.5. Hydrogels are functionalized binding the drug with either an azidoethyl ester bond or an amidic bond, following an innovative synthesis route. After fabrication, release from hydrogel coated microdevices as a function of the environmental pH is characterized. Finally, devices are magnetically actuated and the possibility to achieve spatially and temporally controlled release is demonstrated. The functional microtransporters described in the present work are particularly promising for in-vivo applications in environments where pH differences are present, like the digestive apparatus.

* Corresponding author.
E-mail address: filippo.rossi@polimi.it (F. Rossi).
[1] Equal contribution.

https://doi.org/10.1016/j.matdes.2020.109212

1. Introduction

Routes for medicine administration and their relative pharmacokinetics inside the human body [1–3] are among the most critical topics in modern medicine. Indeed, the efficiency of newly developed therapeutic agents is strongly limited by inefficient administration strategies. Conventional drug delivery approaches are based on the non-selective distribution of the active substance in the whole body mediated by blood circulation [4,5]. By following this route, however, most of the drug is unused, which means that higher dosages must be provided to reach the active concentration in the target organ. This circumstance strongly lowers administration efficacy and intensify drug side-effects. For this reason, recent advanced administration strategies are based on targeted delivery [6–8]. Drugs are released in controlled amounts only in correspondence of the target organ, consequently avoiding indiscriminate distribution across the whole body and limiting the invasiveness of the therapy. A wealth of smart delivery approaches has been described in the literature. Many of them are based on nanometric structures tailored to travel the blood system until they reach the target organ, where they exert their targeted therapeutic action [9]. This is the case of delivery systems based on liposomes [10,11], polymeric micelles [12], nanoparticles [13–15], microspheres [16] and DNA composed nanostructures [17]. Other release modalities use specifically designed polymers to control the release of the drug [18–20]. This is the case of materials like polypyrrole [21,22], hydrogels [23–26] based on chitosan [27] or alginate [28] and many others. Polymers for drug delivery can be easily designed to allow for release in the presence of thermal stimuli [29], pH variations [30–32] or electric fields [33,34]. This is for example the case of alginates, which can be tailored to release the drug only in a well-defined pH range thank to the application of click chemistry [35,36].

Besides the development of new delivery platforms, another promising methodology to address even higher precision drug delivery have been recently developed. This approach is based on the implementation of controlled release materials with wirelessly navigable smalls-scale devices, also known as micro- and nanorobots [37–40]. Small-scale robots have the potential to be remotely guided towards the target organ inside human body and perform localized drug delivery. Since they are intended for in vivo use, their locomotion strategy is a critical point. Even though various remote actuation methods (chemical [41], light [42], ultrasounds [43]) have been proposed, magnetic actuation is the most promising. Magnetic fields interact minimally with living tissues, are able to actuate microdevices with superior precision and can be generated in a highly controlled way [44]. A large number of functional magnetic micro- and nanodevices has been developed in the past to cover application fields such as cell delivery [45], localized surgery [46], bacteria disinfection [47], and also drug delivery [48–52].

The precise delivery of targeted cells through magnetic field–driven microrobots can be addressed by using three-dimensional laser lithography coated with nickel as developed by Sun and coworkers [45]. Nickel helped in magnetic actuation and titanium was inserted to improve biocompatibility for carrying and delivering targeted cells in vivo under a magnetic gradient field-driven mechanism. In a similar direction, stereolithography 3D printing and wet metallization were combined to develop microrobots that showed photocatalytic activity towards water pollutants at low cost [47]. The possibility to coat microrobots with polymeric layers was presented by Ulrich and coworkers [46], which described the use of conductive polymers to coat metallic devices. Following this strategy, ocular microrobots that can be driven wirelessly using an applied magnetic field can be prepared with high potentiality for eye-targeted drug delivery and ophthalmic surgery. Other studies were conducted in similar directions, understanding the role of the device shape in drug delivery performances [49,52] and maintaining high motility and low cytotoxicity of the entire microrobot [51]. The use of these devices, which can be guided by an external magnetic systems, can allow high patient safety (deep penetration and safety of magnetic fields) and minimally invasive nature of the procedure. All the approaches proposed evidenced the use of physical loading of the drug within the external layer, with consequent low drug loading percentage and uncontrolled release rates. A big challenge in material design is represented by the possibility to carry the drug, using magnetic field, without releasing it and addressing a target drug release only in the target site. This approach can guarantee lower concentration of the drug used on one side and, on the other, reduce the drawbacks connected to drug overdosing.

The main idea of the present work is to apply chemically tailored hydrogels, which are able to release a drug in a well-defined pH interval, on existing magnetically actuated microdevices [53]. Such microdevices have been recently manufactured taking advantage of the high flexibility of the microstereolithography (μSLA) technique and the low cost of wet metallization [54]. The combination of these two fabrication technologies also allows for easy and versatile batch production. The devices present a scaffold-like porous structure, primarily intended for cell transportation [53]. Such conformation is, however, ideal also to accommodate hydrogels layers. Internal voids, which completely fill with material, can in fact allow for very high hydrogel loadings on the device. The drug present in the hydrogel is binded to the biopolymer thank to a cleavable bond, which can be broken only in presence of a specific pH range. By doing this, drug release can be programmed to take place only when the device reaches a part of the human body in which that specific pH level is present. Consequently, the approach described in the present work allows two levels of control on the release process of the drug: release is targeted in space, thanks to the possibility to precisely direct the microdevice to the target organ, but also targeted in time, since it takes place only when the device reaches the environment presenting the desired value of pH. Consequently, the drug is not released immediately inside the body but only when the device reaches the suitable environment. The absence of premature leakage during the journey of the microdevice to the target organ enhances its delivery efficacy and prevents potential undesirable side effects to healthy tissues.

2. Experimental section

All reagents were purchased from Merck KGaA (Darmstadt, Germany). Rhodamine derivatives were stored in the dark at 4 °C.

2.1. Chemical characterization techniques

Intermediate and final products were analyzed through FT-IR spectroscopy. FT-IR transmission spectra were recorded using a Thermo Nexus 6700 spectrometer coupled to a Thermo Nicolet Continuum microscope equipped with a 15 × Reflachromat Cassegrain objective at a resolution of 4 cm^{-1}. Samples were prepared as KBr pellet. Absorbance was measured by UV spectroscopy applying the Lambert–Beer method.

2.2. Synthesis of aminoethyl rhodamine 1

Rhodamine (RhB) functionalization with ethylenediamine was performed following the procedures discussed in our previous work [55] and by Mandal's group [56]. Briefly, a solution of rhodamine (600 mg, 1.25 mmol) in ethanol (15 mL) was set and the amine compound (2.73 mL, 40.1 mmol) added dropwise, at room temperature (r.t.). The stirring mixture was heated to reflux for 24 h and then cooled to r.t.; the solvent was removed under reduced pressure and the residue was dissolved in HCl 1 M solution (15 mL) to remove any unreacted ethylenediamine molecules. Successively, NaOH 1 M (23 mL) was slowly added and the resulting precipitate was recovered by filtration, washed with water (3 × 10 mL) and dried to get the final product **1** (Fig. S2). The product was used without further purification. Analytical data were in agreement with literature [57].

2.3. Alginate-RhB functionalization via amidic bond (Alg—Am)

Sodium alginate (200 mg, 0.93 mmol) was dissolved in distilled water (25 mL) and the modified rhodamine **1** (225 mg, 0.46 mmol) was added to the solution at r.t, until complete dissolution. *N*-hydroxysuccinimide (NHS, 26.8 mg, 0.23 mmol) and *N*-(3-dimethylaminopropyl)-*N*′-ethylcarbodiimide hydrochloride (EDC, 44 mg, 0.23 mmol) were added, and the resulting system was left stirring for 12 h. The functionalized polymer was purified by dialysis against aqueous solution (2 L of distilled water and 11.2 g of NaCl) to remove unreacted chemicals and salts. Dialysis was performed using regenerated cellulose membrane (M_w cut-off 3.5 kDa) for 2 days, by replacing the aqueous solution with distilled water after the first 24 h. The product was collected as pink solid after lyophilization. It is referred as Alg-Am (Fig. S2).

2.4. Synthesis of 3-azido-1-propanol 2

3-chloro-1-propanol (0.88 mL, 10.58 mmol) was dissolved in DMF (20 mL) and sodium azide (0.79 g, 12.16 mmol) was progressively added; the resulting system was heated up to 50 °C and kept stirred for 24 h. Successively, the mixture was diluted with brine solution and extracted with diethyl ether (2 × 25 mL). The resulting organic phase was washed in brine (5 times) and finally dried over anhydrous sodium sulfate, filtered and concentrated under vacuum to obtain product **2** (Fig. S3).

2.5. Synthesis of rhodamine azidoethyl ester 3

In CH_2Cl_2 (5 mL), the following reagents were sequentially added: RhB (300 mg, 0.63 mmol), compound **2** (82 mg, 0.81 mmol), EDC (132 mg, 0.69 mmol) and 4-dimethylaminopyridine (DMAP, 15.4 mg, 0.125 mmol). The mixture was left stirring for 4 h, at r.t. avoiding direct light exposure. Then, CH_2Cl_2 (10 mL) was added and the organic solution washed with distilled water (2 × 10 mL), HCl 0.1 M (2 × 10 mL) and finally brine solution (2 × 10 mL). The collected organic phases were dried over anhydrous sodium sulfate and filtered; the solvent was removed under reduced pressure affording the desired product **3** (Fig. S3) without further purification. Analytical data were in agreement with literature [58].

2.6. Synthesis of alkyne modified alginate 4

Sodium alginate (1 g, 4.63 mmol) was dissolved in distilled water (40 mL) and propargylamine (118 μL, 1.85 mmol) was added dropwise. A solution of 1-hydroxybenzotriazole hydrate (250 mg, 1.85 mmol) in acetonitrile:water 1:1 v/v (15 mL) at 40 °C was poured to the polymer solution and, subsequently, EDC (353 mg, 1.85 mmol) was added. The resulting mixture was stirred for 24 h at r.t. It was then dialyzed against acid aqueous solution pH = 5.5 (2 L of distilled water dissolving 11.2 g of NaCl and 4 drops of HCl 37% w/w). Dialysis (membrane M_w cut-off 3.5 kDa) occurred for 4 days, with daily water changes and addition of HCl 37% w/w. Finally, the solution was stored at −80 °C and lyophilized to obtain product **4** (Fig. S3).

2.7. Alginate-RhB functionalization via click chemistry

The "click" reaction used to conjugate products **3** and **4** was the copper(I)-catalyzed alkyne-azide cycloaddition (CuAAC) as visible in Fig. S3. **4** (125 mg, 0.5 mmol) was dissolved in distilled water (10 mL), whereas **3** (104.5 mg, 0.2 mmol) was added to a solution of THF: water 1:1 v/v (4 mL). The latter was mixed to the former and copper iodide (5.7 mg, 0.03 mmol) and sodium ascorbate (6 mg, 0.03 mmol) were added. The system was left stirring for 24 h at 60 °C. The resulting solution was dialyzed as discussed for modified polymer **4** to remove the excess reactants and byproducts. The final product was obtained as purple solid after lyophilization. It is referred to as Alg-Es-Tr (Fig. S3).

2.8. Microdevices production

Porous gold coated microrobots were manufactured following the procedure presented in our previous paper [53], where more information about the production route can be retrieved. Briefly, they were designed using Solidworks and 3D printed using a stereolithography machine. After the 3D printing process, their surface was cleaned and etched with an alkaline KOH solution. Subsequently, the surface was activated with Pd and electroless coated with an alkaline formaldehyde-free copper solution. After Cu, CoNiP was applied using an alkaline solution. This layer was followed by a NiP coating, which was employed as base layer for deposition of the final gold layer by galvanic displacement. Fig. S1 depicts the appearance of uncoated samples.

2.9. Alginate-based hydrogel coating

Metal coated devices were dipped in alginate-based water solution (1% w/v) for 20 min in ultrasound bath. Then devices were dipped in $CaCl_2$ (5% w/v) water solution with final alginate gelation. This procedure can be repeated to increase the hydrogel coating thickness. In drug delivery experiments drug mimetic (RhB) was dissolved in alginate aqueous-solutions and the procedure was maintained the same.

2.10. Magnetic actuation

Magnetic actuation was performed employing a coils array known as the Octomag [59] (Fig. S7). Devices were magnetized placing them on a cylindrical NdFeB permanent magnet. Such magnet was 2 cm (radius) × 1 cm (thickness). Samples were carefully removed after the magnetization. Devices speed was calculated actuating the devices in a small basin filled with water and analyzing the videos acquired with a tracking software. For targeted actuation, a custom-made test channel was carved in polycarbonate employing a numerical control cutter. Its dimensions are detailed in Fig. S8.

2.11. In vitro drug delivery and mathematical modeling

Drug release mechanism was investigated in simulated physiological conditions: at 37 °C and 5% CO_2, in a phosphate buffered saline solution (PBS, pH 7.4) and in acidic condition (pH = 4.5). In details, each device was placed in excess of PBS (2.5 mL) and aliquots were collected at defined time points, replacing them with an equal volume of fresh solution, in order to preserve the diffusion regime among the nanosystem and the release environment. Percentages of released RhB were then measured by UV spectroscopy at a specific wavelength, respectively 485 nm and 570 nm. Drug diffusion mechanism can be described as 1-dimensional model of the second Fick law where the device geometry is a cylinder and the material flux mainly takes place at the PBS/hydrogel surface. Eq. (1) showed these considerations, indicating r as the characteristic radius for the mass transport phenomenon. The following mass balance equations are written considering the variation of the mean drug concentration within the hydrogel (C_G) related to the volume of solution (V_S), the mean drug concentration in the outer solution (C_S), the total volume (V_G), the NGs mass present inside the matrix (m_G) and the exchange interfacial surface (S_{exc}), that represents the boundary surface between hydrogel and surrounding solution (which, simplifying, can be here considered as being only the side surface). According to these expressions, the boundary conditions are defined describing the profile symmetry at the center of the polymeric cylinder, with respect to the radial axis of the cylinder (Eq. 5) and the equivalence between the material diffusive fluxes at the PBS/hydrogel surface (Eq. 6).

$$\frac{\partial C_G}{\partial t} = D \cdot \frac{1}{r^2} \cdot \frac{\partial}{\partial r} \cdot \left(r^2 \cdot \frac{\partial C_G}{\partial r} \right) \tag{1}$$

$$V_S \frac{\partial C_G}{\partial t} = k_C \cdot S_{exc} \cdot (C_G - C_S) \quad (2)$$

$$C_S(t=0) = 0 \quad (3)$$

$$C_G(t=0) = C_{G,0} = \frac{m_{G,0}}{V_G} \quad (4)$$

$$\left.\frac{\partial C_G}{\partial r}\right|_{r=0} = 0 \quad (5)$$

$$-D \cdot \left.\frac{\partial C_G}{\partial r}\right|_{r=R} = k_C \cdot (C_G - C_S) \quad (6)$$

This mathematical model allowed to estimate the diffusion coefficient (D) of RhB, in order to evaluate the influence of the alginate functionalization on the drug release. Sherwood number obtained by means of penetration theory allowed the computation of the mass transfer coefficient k_C (Eq. 7).

$$Sh = 1 = \frac{k_C \cdot 2r}{D} \quad (7)$$

3. Results and discussion

3.1. Drug-hydrogel conjugates synthesis

To improve the performance of drug delivery through hydrogel coatings we functionalized alginate in order to create a pH-sensitive linker between polymeric network and drug molecules. Two strategies were investigated: the synthesis of an ester bond-based and an amide bond-based cleavable linker. In general, the former could be gradually hydrolyzed in physiological environment via a pathway generally recognized as "catalyzed by water-derived ions" [60] and it is decomposed by strong acids and bases [30]; whereas amide bond presents an improved chemical stability in water and its cleavage is possible only with stronger pH variations [61]. Due to the alginate chemical structure, the ester functionalization was carried out with the aid of click chemistry: RhB (chosen as drug mimetic) was modified with azide group through esterification (RhB azidoethyl ester), whereas the alkyne moiety was grafted to the polymer chains. The copper(I)-catalyzed alkyne-azide cycloaddition occurred in the formation of the 1,4-disubstituted triazole, a stable and uncleavable bond [62], and gave rise to the final functionalized structure polymer-drug (hereinafter Alg-Es-Tr, referring to the combination of ester and triazole bond between alginate and RhB). The reactions involved in this strategy are reported in Fig. S2 and S3. On the other side the alginate amide modification was performed through the synthesis of aminoethyl RhB and the reaction of the latter with the polymer carboxyl groups. The resulting product was labeled as Alg-Am and the corresponding synthesis pathway is showed in Fig. S2. The alginate functionalizations via click chemistry and amidation were performed with a non-stochiometric ratio between the reagents to maintain some of carboxyl groups. In this way, the latter were jointed to the calcium cations creating cross-linking points and forming the gel scaffold. FT-IR spectra show the characteristic peaks of the modified moieties compared to the pristine polymer.

Sodium alginate (Fig. S4A) presents well detectable signals related to its hydroxyl, ether and carboxyl groups: the broad transmission band around 3430 cm^{-1} represents the -OH stretching, whereas the signal at 2920 cm^{-1} is due to the aliphatic C–H stretching vibration; the carboxylate anions generate asymmetric and symmetric stretching respectively around 1620 cm^{-1} and 1420 cm^{-1}. The chemical structure of the polysaccharide highlights other peculiar peaks in the wavenumbers range 1295–940 cm^{-1}: C–O stretch at 1295 cm^{-1}, 1183 cm^{-1} and 940 cm^{-1}, C–C vibration (stretching) is showed at 1110 cm^{-1} and the C-O-C stretching is assigned at 1029 cm^{-1}. Referring to click chemistry strategy, the FT-IR spectrum of modified alginate with alkyne groups (Fig. S4B) confirms the triple bond functionalization due to the appeared signals around 3280 cm^{-1}, related to the terminal methyne stretch, and at 2119 cm^{-1} indicative of the C≡C stretching vibrations. The cycloaddition alkyne-azide to synthetize the alginate-RhB derivative can be evaluated in the corresponding FT-IR spectrum (Fig. S4D). Here, the alkyne signals disappear, whereas the new peaks at 1747 cm^{-1} (shoulder signal), 1727 cm^{-1}, 1714 cm^{-1} are representative of the triazole linker. Moreover, the spectrum compared with that of RhB azidoethyl ester shows the absence of the azide signal at 2090 cm^{-1} and, in the range 1500–700 cm^{-1}, the peaks related to RhB are detectable and matched (Fig. S4C). Regarding the formation of amide linker, FT-IR spectrum of RhB amine derivative (Fig. S5F) shows the characteristic peaks of N–H symmetric and asymmetric stretching at about 3448 cm^{-1} and 3380 cm^{-1}, the C=O stretching at 1685 cm^{-1}, the amine bending at 1616 cm^{-1} and the C–N absorption band at 1218 cm^{-1}. The other signals in the wavenumbers range 1650–700 cm^{-1} are representative of the chemical structure of RhB, pointing out the stretching vibration of C–C in aromatic rings at 1515 cm^{-1} and the in-plane C–H bending around 1116 cm^{-1} [63,64]. The formation of amidic bond between alginate and aminoethyl RhB can be confirmed by the peculiar signals in the corresponding IR analysis (Fig. S5E): the signal around 3190 cm^{-1} is indicative of the N–H stretching band, whereas the C=O stretching (amidic band I) is detectable at 1675 cm^{-1} even if partially covered by the alginate COO^- vibrations.

The N–H bending (amidic band II) is estimated at 1554 cm^{-1} (shoulder signal), but it is almost totally overlapped by the C=O band. Finally, in the range 1550–700 cm^{-1} peaks related to RhB aromatic and aliphatic moieties are detectable according to the signals of the FT-IR spectrum of aminoethyl RhB.

3.2. Devices design and manufacturing route

Modified and unmodified hydrogels were applied on suitably designed microdevices to allow for targeted drug release. The main guidelines for the manufacturing of the devices are three: a) biocompatibility, b) magnetic actuability, c) hydrogel loading optimization. To satisfy these requirements the microdevices must present, respectively, the following features: a) a chemically inert surface, b) a suitable metallic coating able to react to the presence of an external magnetic field, c) a scaffolded structure able to accommodate sufficient hydrogel mass and to maximize the ratio between the total usable hydrogel weight and the weight of the device. Considering these requirements, we decided to employ the 3D printed magnetically steerable microscaffolds (Fig. S1) recently developed by our group [53]. These devices were originally designed for cell transportation, but their unique properties of high surface area and biocompatibility allows for their use as multipurpose platforms. Their porous structure can be used to accommodate a large quantity of hydrogel with respect to their volume. Furthermore, pores allow to tune the release, as the drug incorporated inside the device diffuses out in more time with respect to the drug in the hydrogel layers at the surface. Finally, microscaffolds biocompatibility is proved thanks to a MTT assay test performed with mice fibroblasts [53]. For these reasons, they were selected as microrobotic platforms for drug delivery applications. Fig. 1 depicts the manufacturing route followed in the work, with the two initial steps being μSLA printing (Fig. 1a) and wet metallization of the devices (Fig. 1b) according to our previous paper [54]. In particular, four metallic layers were deposited on the surface: an initial copper layer, a CoNiP layer to impart magnetic properties, a NiP layer and a Au layer to provide biocompatibility. Subsequently, two types of RhB loaded hydrogels were deposited by immersion on these devices to obtain the drug releasing microrobots. In one case, RhB was simply dissolved in the alginate solution (Fig. 1c).

In the second case, RhB was chemically binded to the structure of the alginate (Fig. 1d), either with an ester or an amide bond. These two

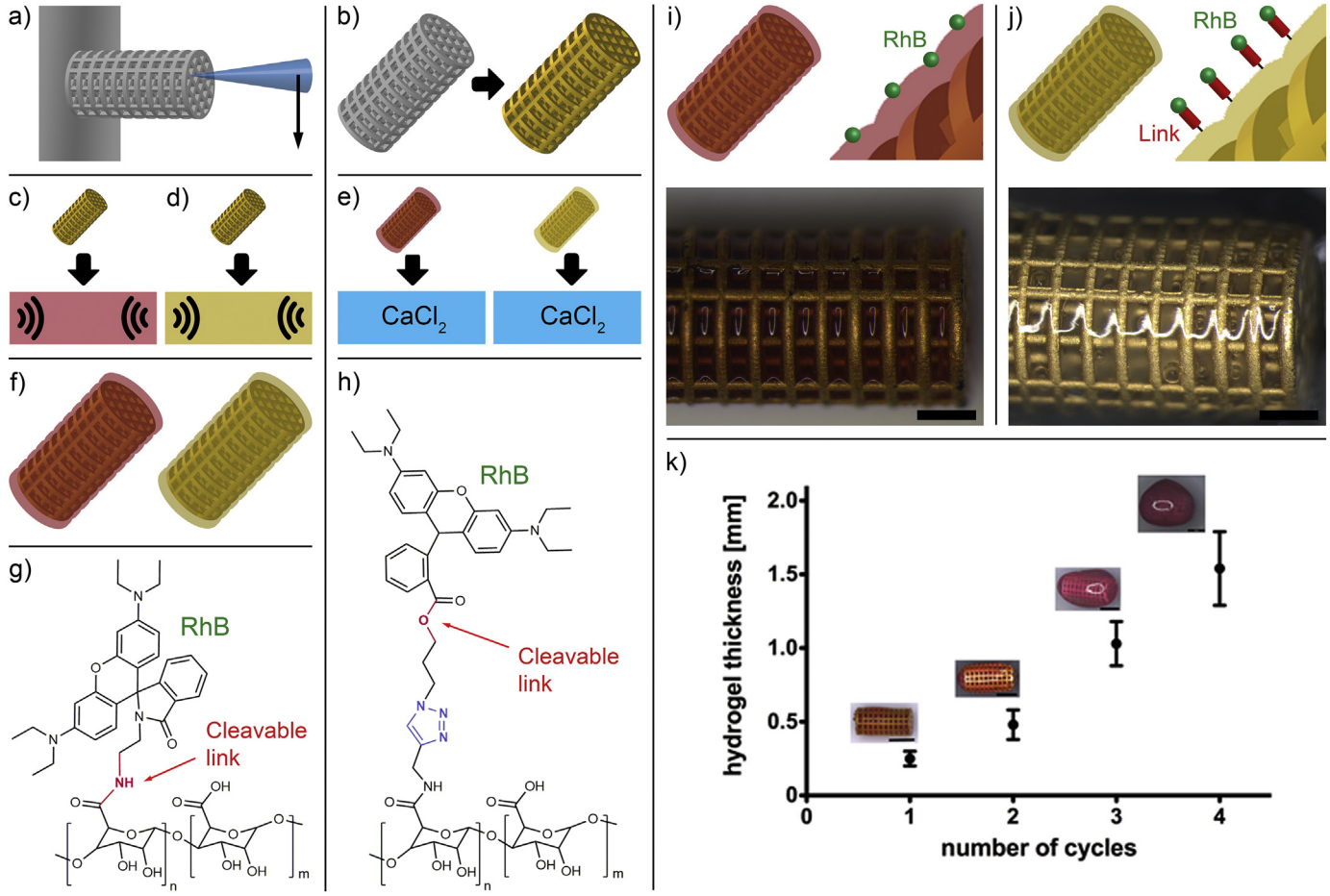

Fig. 1. Production steps for hydrogel coated microrobots: stereolithography 3D printing (a); devices wet metallization (b); device dipping in RhB dissolved in alginate solution in ultrasound bath (c); device dipping in functionalized alginate solution in ultrasound bath (d); hydrogel gelation dipping in $CaCl_2$ water solution (e) to obtain final coated devices (f). Chemical structure of the amide functionalized hydrogel (g). Chemical structure of the ester group functionalized hydrogel (h). Final samples with conceptual models for non-functionalized (i; scale bar = 500 μm) and functionalized (j; scale bar = 500 μm) hydrogels. Hydrogel thickness depending on number of ultrasound-based cycles of sodium alginate and calcium chloride (k; scale bars = 2 mm).

approaches yielded devices containing unbinded and chemically binded RhB, identified as M-NB and M-B respectively. After immersion in the alginate, both samples were immersed in a calcium chloride solution (Fig. 1e) to allow complete gelation. After this step, final M-NB and M-B (Fig. 1f) devices were obtained. M-NB devices contain only physically trapped RhB, while M-B devices contain either Alg-Am (Fig. 1g) or Alg-Est-Tr (Fig. 1h) hydrogel. Fig. 1i and j depict in a clearer way the design principle at the base of the two types of hydrogels. In one case (M-NB) the drug, in this case the widely used model molecule RhB, is not bound to alginate polymeric chains (Fig. 1i) and it is free to diffuse within the polymeric matrix. This implies that RhB release from the alginate takes place purely via diffusion and that it starts immediately in the presence of a concentration gradient. In the case of M-B devices, the drug is grafted to the alginate chain via a cleavable link (Fig. 1j), which can be easily dissolved in a predefined pH range. This renders the release insensitive to concentration gradients and makes possible drug delivery only when the device reaches an environment characterized by the correct pH.

The thickness of alginate hydrogel, presented in Fig. 1k, can be tuned increasing the number of ultrasound-based cycles of sodium alginate and calcium chloride (by sequential deposition of hydrogel multilayers). Drug loading efficiency was calculated and it was found to depend on the number of coating cycles performed. This parameter can be calculated as the ratio between the drug entrapped within the device and the initial amount of drug. In the case of a single layer, RhB loading efficiency was 72.3%, in the case of two layers 64.7%, in the case of three layers 51.9% and in the case of four layers 39.6%. As a consequence of the surface tension of the hydrogel deposited on non-reticulated surfaces, devices coated with many layers appear structurally distorted (Fig. 1k). From the applicative point of view, the presence of more than one layer considerably enhances the quantity of drug carried. However, a distorted structure is not optimal for actuation, since it may result in uncontrolled motion. For this reason, a single coating cycle was employed as tradeoff between shape and hydrogel thickness.

Application of ultrasounds during immersion in the first hydrogel solution allowed for a good penetration of the material inside the porous structure of the devices. Fig. 1i depicts the appearance of a device coated with a single layer of non-functionalized hydrogel, while Fig. 1j shows the appearance of a device coated with a single layer of functionalized alginate. In the first case, since the molecule is not bound to the polymer chain, the typical color of RhB is clearly visible. In the second case, the hydrogel presents a golden color, indicative of the presence of bound RhB.

3.3. Drug delivery performances

Once proved that the alginate hydrogel systems can be successfully functionalized with cleavable bonds (Alg-Es-Tr and Alg—Am) and applied to magnetically steerable microdevices, RhB release was investigated and compared with the case of solute only physically entrapped within the three-dimensional polymeric network. This study is necessary to investigate the benefits related to the use of cleavable linkers

in our hydrogel systems. Release studies were conducted at 37 °C at different pH: 7.4 and 4.5 on M-NB and M-B devices. The percentage of RhB released was defined as the ratio between the released amount in the aqueous media and the total amount linked to the polymeric scaffold.

In Fig. 2a, release profiles at pH = 7.4 associated to Alg-Am and Alg-Est-Tr functionalization were compared with RhB physically entrapped within three-dimensional polymeric network: it is well visible that RhB release profile from alginate is very fast and it is almost completed in the first 2 h, while the release from functionalized system is not observable. In Fig. 2b release kinetics at pH = 4.5 of the three systems are plotted: RhB physically entrapped maintained the same trend while big differences are visible for amide and click-based functionalization.

In particular it is evident that this system is pH sensitive and, in particular, the presence of acidic pH improved the cleavability of the bond with higher percentages of release: amide bond is more cleavable. There the influence of the system in delivering rhodamine was investigated plotting release percentage against time square root (Fig. 2c, d). A linear plot is indicative of Fickian diffusion and the y-axis intercept value an indication of burst release, where it is well known that an ideal controlled release system should present linear trend during time and its y-axis intercept equal to zero. RhB directly loaded within alginate hydrogels shows a linear trend only in the first 4 h and then a plateau trend is visible. Moreover, in this case the burst release contribution is high (about 40%), underlining the expected poor ability to control release of small drugs. On the other hand, loading RhB through ester-click or amide functionalization within alginate hydrogels increases performances in terms of pure diffusive mass transport and in term of burst release contribution that results to be extremely low at pH = 7.4. In acidic conditions linear trend is visible with burst release underlying the high pH-dependence of this system.

In summary, at the beginning (when RhB-loaded devices are placed in the releasing medium) there is a burst release, which corresponds to a very fast discharge of drug driven by the high concentration gradient. As mentioned earlier, its value is about 40% for specimens containing RhB physically entrapped (in both acidic and neutral pH), 36% for Alg-Am and 32% for Alg-Est-Tr (at acidic pH). Note that at neutral pH, burst release is absent for specimens where RhB is covalently linked to the hydrogel chains. Burst release is followed by a linear release of drug with time, which corresponds to a pure Fickian diffusion [65] and is only driven by the concentration gradient. Finally, the release

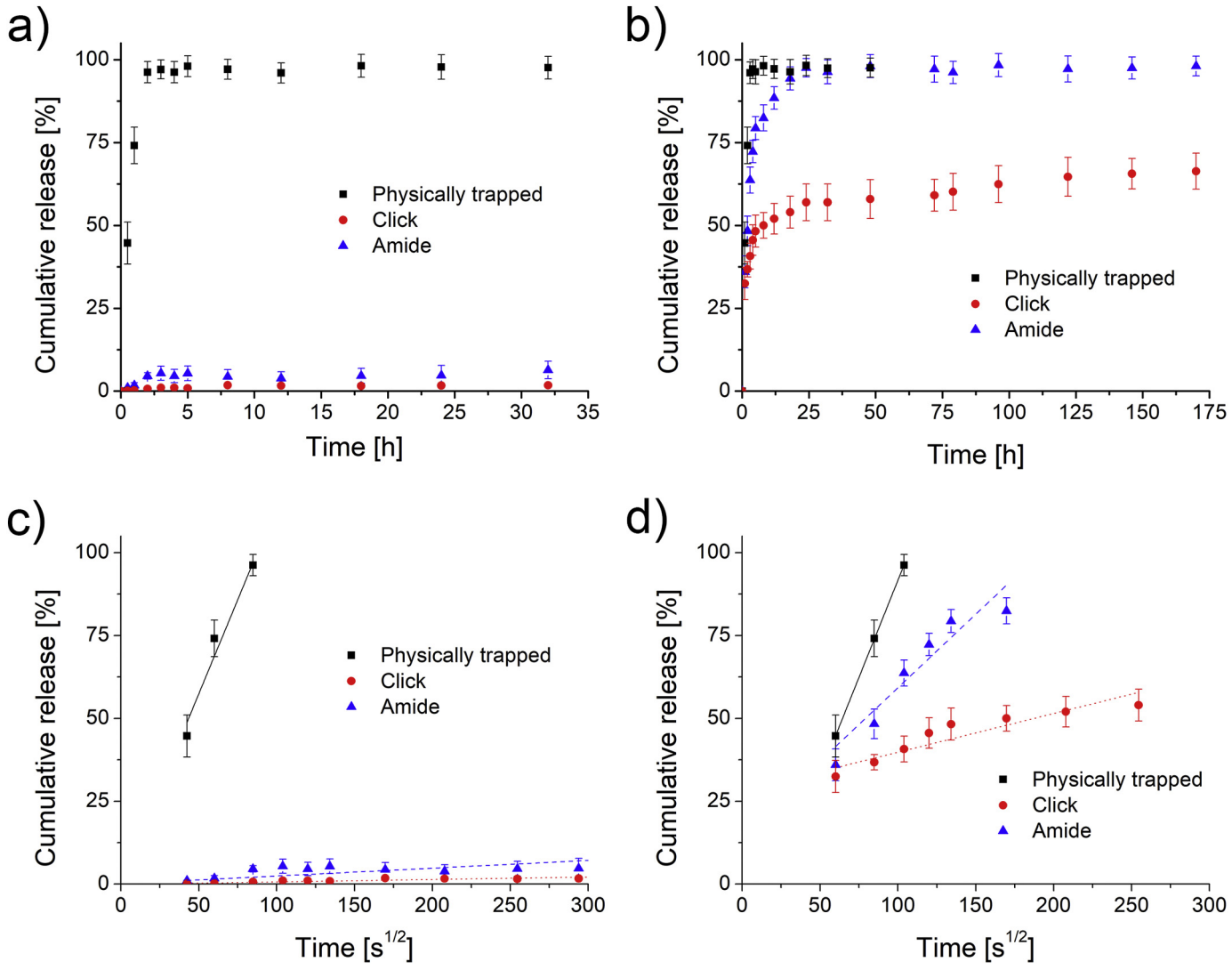

Fig. 2. (a) In vitro release profile at pH = 7.4 of RhB delivered from alginate only physically entrapped, Alg-Am (Amide) and Alg-Est-Tr (Click) functionalized hydrogels. (b) In vitro release profile at pH = 4.5 of RhB delivered from alginate only physically entrapped, Alg-Am (Amide) and Alg-Est-Tr (Click) functionalized hydrogels. (c, d) The slopes of the RhB release from corresponding alginate hydrogels against the square root time. The slope of the rhodamine release from hydrogels against the square root time is representative of the Fickian diffusion coefficient of rhodamine in gels ($p < 0.0001$ between all of the groups). The values are calculated as a percentage with respect to the total mass loaded (mean value ± standard deviation is plotted).

Table 1
Diffusion coefficient of RhB in alginate hydrogels.

	Diffusivity [cm^2/s]	
	pH = 7.4	pH = 4.5
Physically entrapped	$2.6\ 10^{-4}$	$2.8\ 10^{-4}$
Alg-Est-Tr	/	$4\ 10^{-6}$
Alg-Am	/	$5.7\ 10^{-5}$

curve exhibits a plateau trend. After the release mechanism is completed, the remaining drug entrapped within the hydrogel network is released until the complete degradation of the entire network. In our study, pure Fickian diffusion takes place only for up to 3 h for specimens where RhB is only physically entrapped, while it takes 8 h for Alg-Am and 18 h for Alg-Est-Tr. However, the final aim of this device is not to prolong the release of drugs for long times, but enable the selective release of drugs by exploiting a stimulus such as pH present within the body.

Mass release data obtained experimentally (Fig. 2), were used to estimate the model drug diffusion coefficients. As explained above, the release mechanism could be considered as a pure Fickian diffusion, being concentration driven through alginate hydrogel pores. Table 1 shows the dependence of RhB diffusivity on pH. It is well visible that RhB only physically entrapped evidenced no differences in diffusivity. Among different functionalizations it is observable that at pH = 4.5 Alg-Est-Tr hydrogels showed lower diffusion coefficient related to the cleavability of the bond.

It is useful to highlight that, thanks to their design, devices can be reused at the end of the first drug delivery cycle. Since the base of the device is a rigid 3D printed and wet metallized structure, exhaust hydrogel can be removed simply by immersion in a solution containing a weak acid (like citric acid). After this step, devices can be coated again with a new hydrogel layer.

3.4. Magnetic actuation

Microdevices described in the present paper were actuated employing a rolling motion approach [47,53]. The working principle for this kind of actuation is the application of a magnetic torque on the device thanks to the presence of the magnetic CoNiP layer. Eq. 8 describes the torque obtainable on a sample immersed in a magnetic field.

$$\overrightarrow{T_m} = V \cdot \vec{M} \times \vec{B} \tag{8}$$

V is the volume of magnetic material, M is the magnetization of the material and B is the external applied magnetic field.

The torque applied depends thus on the volume of magnetic material present, e.g. the thickness of CoNiP, its magnetization and the intensity of the external magnetic field. To correctly actuate it, the device must present a permanent magnetization M perpendicular to its major axis. This is the rationale for the use of CoNiP as magnetic alloy, since this material presents a semi-hard magnetic behavior. In absence of a permanent magnetization, the device simply aligns with the

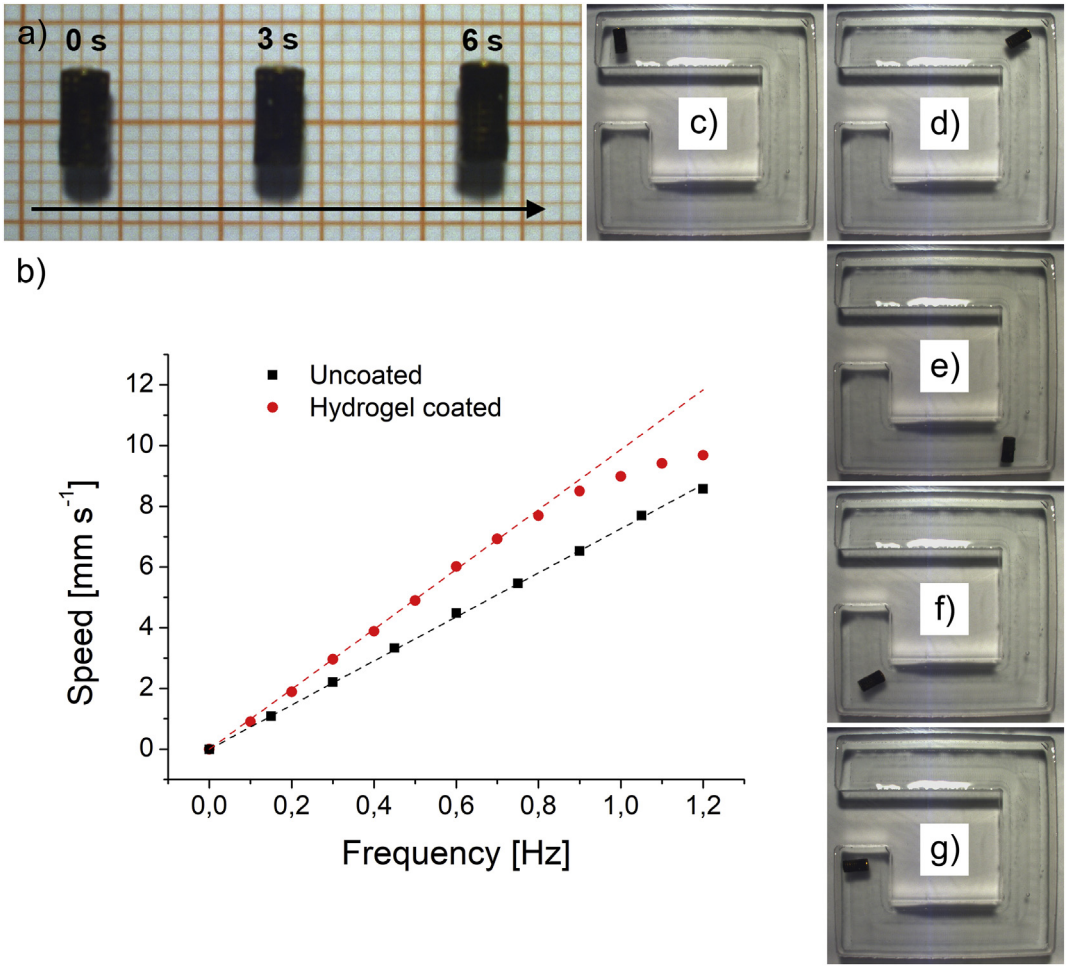

Fig. 3. Magnetic actuation of hydrogel coated microdevices: linear actuation at constant time intervals (a); speed vs. frequency plot for devices coated with two steps of hydrogel (b); actuation of a M-B device inside a water filled test basin (from c to g).

external magnetic field along its easy axis, which corresponds to its major axis. In this case, the torque applied is perpendicular to the axis itself, resulting in an unwanted rotation movement. CoNiP deposited on the samples (Fig. S6) was characterized by remanence levels as high as 140 emu cm^{-3} in the direction parallel to the symmetry axis and 96 emu cm^{-3} in the direction perpendicular to the same axis [53]. Moreover, the material must not lose easily its magnetization when exposed to external magnetic fields. For this reason, relatively high coercivities are required. Also in this case CoNiP is a good choice thanks to its coercivity higher than 600 Oe along any direction [53]. To provide magnetization M, the samples were placed in contact with a strong NdFeB permanent magnet. Subsequently, they were placed in a setup (Fig. S7) able to provide highly controlled magnetic fields, called Octomag [59]. Such setup can apply magnetic gradients, rotating and oscillating fields according to 5 degrees of freedom. Obviously, the intensity of the torque is maximum when the angle between the directions of M and B is 90°, while is 0 when such angle is 0°. This implies that, when subjected to the external magnetic field, the device aligns its magnetization vector with the direction of B thank to the torque applied on the device itself. If B continuously rotates around an axis, M will continuously align with B. This generates a continuous torque that rotates the microrobot around its cylindrical axis. The final result, when placed on a solid substrate, is that the contact with the material generates a net forward motion like in the case of a wheel. Fig. 3a depicts a M-B device immersed in water on a glass surface that moves at constant speed. Intuitively, since the devices are equivalent to wheels, the speed obtained is correlated to the rotation frequency of the external field by eq. 9.

$$v = 2\pi r\omega \tag{9}$$

Where r is the radius of the device and ω is the rotation frequency of B. If M follows B in an ideal way, this correlation is expected to be linear. Deviations from linearity can however be possible if M follows B with a certain delay, as expectable the case of viscous solutions exerting a considerable fluidodynamic drag on the devices. Microdevices not covered by hydrogel were found to be moveable with great precision upon application of an external magnetic field [53]. Fig. 3b depicts the correlation between the rotation frequency of B and the speed of the device obtained in water. Such correlation was found to be linear in the range of frequencies considered and the experimental points were fitted using equation n. The fitting allowed to evaluate indirectly the radius of the devices, which was found to be 1156 μm. This value is close to the nominal one (1200 μm) expected from 3D printing. After hydrogel application, however, external diameter and weight of the devices significantly change. To investigate the effect on microrobots speed and general behavior, linear actuation tests were performed at increasing rotation frequencies of the applied field. The result obtained is visible in Fig. 3b. The most important effect of hydrogel addition is the introduction of a non-linear behavior at high actuation frequencies. When rotation frequency exceeded 0.8 Hz, behavior was found to deviate from the linear relationship described by equation n. Speed values where found to be lower than expected ones. The main reason for this behavior can be the weight of the device, which increased by 80% with the addition of the hydrogel layer. It is also possible that hydrogel coated microrobots mechanically interact with the substrate in a way different with respect to uncoated devices. In particular, friction coefficient can be significantly lower. The linear part of the curve visible in Fig. 3b was linearly fitted to evaluate the radius of the devices. A radius of 1570 μm was evaluated, with a 414 μm difference with respect to the uncoated sample. Such difference corresponds to the mean thickness of

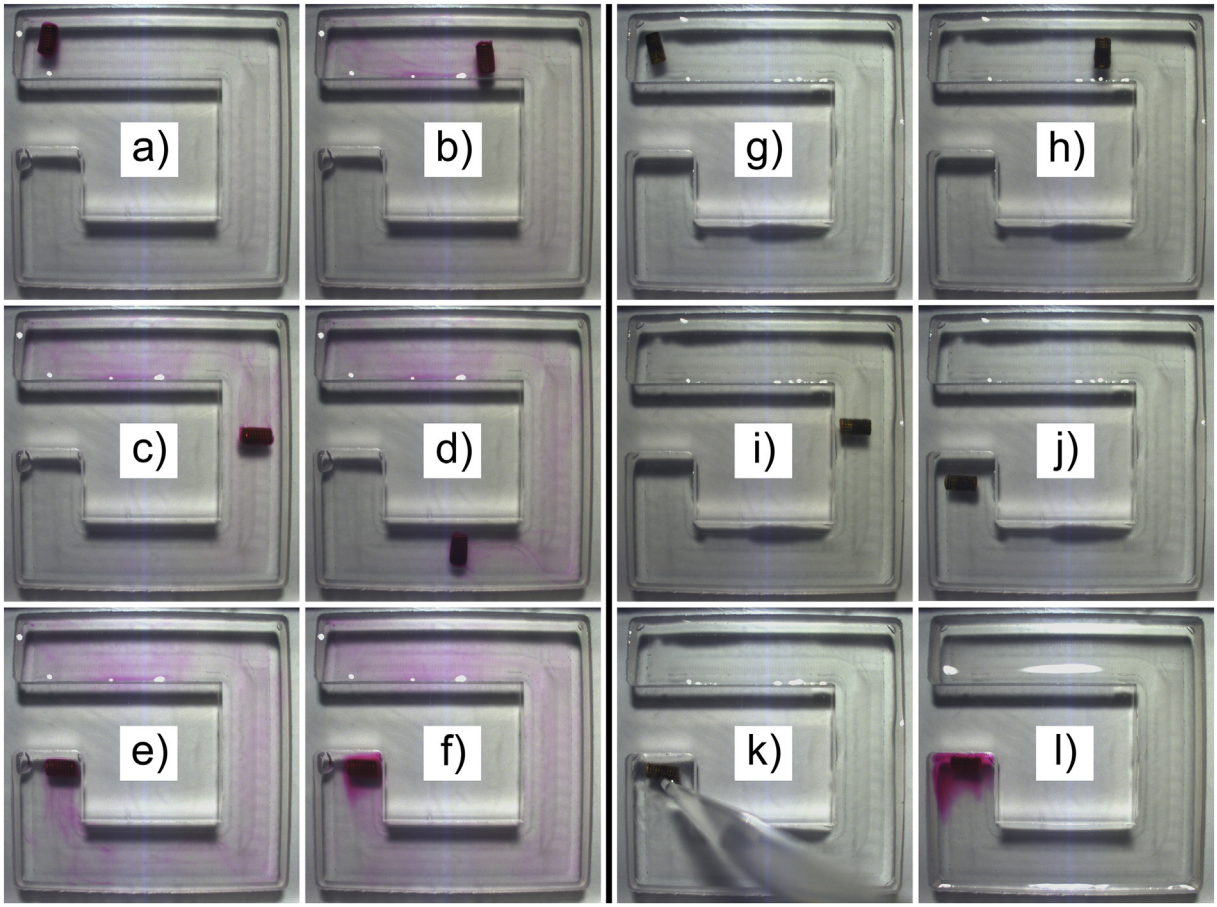

Fig. 4. Targeted RhB release tests from a M-NB device (from a to f) or from a M-B device (from g to l).

the hydrogel on the outer zone of the microrobot. Obviously, the distribution of the hydrogel is not perfectly uniform. For this reason, the value obtained must be considered and indirectly measured mediated value.

As demonstrated in our previous work, devices can be easily steered by varying the inclination of the rotation axis of the applied field B (Supporting Video 1 reports the case of a device performing a series of 90° turns, while Supporting Video 2 depicts a device following a circular pattern). By doing this, the devices can be efficiently guided towards the target inside complex shaped environments, as evidenced in Fig. 3c - 3 g in the case of a custom made test basin. Such basin was characterized by the dimensions reported in Fig. S8 and was filled with deionized water. To follow the shape of the test basin, inclination of the rotation axis was sequentially changed by 90°, keeping constant the rotation frequency of B. Initially, the device moved towards the right until the first turn (Fig. 3c). Then, the rotation axis of the magnetic field was turned clockwise by 90° (Fig. 3d).

The same procedure was repeated in correspondence with the second (Fig. 3e) and the third turn (Fig. 3f) until the device reached the target zone (Fig. 3g).

3.5. Targeted drug delivery

To test the possibility of pH triggered drug delivery from the biocompatible and dimensionally stable (Fig. S9 and S10) hydrogel coated microrobots obtained, we employed the same test basin depicted in Fig. 3 with the same actuation pattern. In this case, the target zone at the end of the channel represents the target organ for drug release. Consequently, drug delivery should preferentially take place exclusively in correspondence of the target zone. In the first tests performed, a M-NB sample was guided towards the target zone. Fig. from 4a to 4f and Supporting Video 3 depict the result obtained. As expected, the device immediately started releasing RhB from the moment it came in contact with the water (Fig. 4a). During motion (Fig. from 4b to 4e), it left a clearly visible trace of RhB stained water. When it reached the target zone, it continued to release RhB (Fig. 4f was acquired after 60 min). Obviously, by using unbound RhB, a non-negligible amount of the chemical was released in zones of the basin far from the target zone. This implies a considerable waste of drug, which would be released in unwanted zones of the organism in the case of a real application.

In the second test, a M-B sample was employed. As clearly evidenced in Fig. from 4 g to 4 l and Supporting Video 4, release took place only in the target zone. No unwanted release was observed when the device was placed in the water (Fig. 4g) and when it was guided towards the target zone (Fig. from 4 h to 4j). To obtain the correct pH conditions, 200 μL of a 1 M sulfuric acid solution were pipetted in correspondence of the device (Fig. 4k). This procedure, which was adopted for practical reasons, is representative of an equivalent case in which a device reaches a region of the channel already characterized by low pH. The pH variation induced by the presence of the acid immediately triggered RhB release due to cleavage of the corresponding bond. As a consequence, the target zone was readily colored by released RhB after 60 min from the acid addition. Contrarily to the M-NB sample, with M-B it was possible to limit the release to the target zone, avoiding premature RhB release in other zones of the basin.

4. Conclusions

The possibility to carry drugs, using magnetic field, without releasing it and addressing a target pH-dependent drug release only in the target site is an extremely promising medical strategy. The main advantages reside in the possibility to consent the use of less amount of drug with consequent reduced drawbacks connected to drug overdosing. Here two strategies were followed to prepare pH-controlled drug releasing hydrogels. In the first case, the model molecule Rhodamine B was linked to the alginate polymeric chain with a cleavable ester bond. In the second material, an amide bond-based cleavable linker was employed. These hydrogels, as demonstrated by the tests performed, presented a negligible release for pH higher than 4.5. In comparison, in the same pH range, hydrogels containing non-bonded Rhodamine were characterized by very fast release kinetics. For pH environments around 4.5, functionalized hydrogels started releasing Rhodamine B with kinetics considerably slower than the equivalent non-functionalized material. Indeed, the Alg-Est-Tr hydrogel was characterized by a diffusion coefficient equal to $4\ 10^{-6}$ cm^2/s, while the Alg-Am hydrogel presented a coefficient equal to $5.7\ 10^{-5}$ cm^2/s. Both values are significantly lower than the one observed in the case of physically trapped RhB ($2.8\ 10^{-4}$ cm^2/s). This result demonstrated the possibility to switch on the release by varying the pH of the environment, allowing for a temporal control over drug delivery. Such temporal control was advantageously coupled with a complementary spatial control by applying the hydrogel on wirelessly controlled microdevices. This result was achieved employing porous microrobots presenting a gold coated surface. Hydrogels were successfully applied on their surface by immersion, filling the structure of the devices. Hydrogel coated microrobots were then magnetically actuated to evaluate controllability of their speed and position. Higher speeds (up to 10 mm/s) were observed as a consequence of the increased diameter of the device after application of the alginate layer. Moreover, coated devices deviated from linearity at higher frequencies with respect to uncoated ones. High precision control was demonstrated successfully guiding the microrobots inside a narrow test channel. To demonstrate controlled drug release, two devices were guided in the same channel and allowed to release Rhodamine B close to the end of the channel itself. In the case of the device covered with non-functionalized hydrogel, release was found to start immediately upon immersion in the channel. This implied a considerable waste of drug along the path to reach the final part of the channel. Contrarily, functionalized hydrogel coated microrobots did not release Rhodamine B during the travel to reach the end of the channel. Conversely, they released the dye when the environment was locally modified decreasing its pH. In this way, Rhodamine B was released only in correspondence of the end of the channel. Considering these results, it is evident that functionalized hydrogel coated microdevices may be potential candidates to perform targeted drug delivery in environments where pH differences are present. A typical example is the digestive apparatus, which is characterized by pH levels ranging from acidic to mildly alkaline. It is therefore possible to design the cleavable link between the drug and the alginate to allow release in correspondence of the target region of the digestive system. The microrobots carrying the corresponding functionalized alginate may therefore cross non-target zones of the apparatus without releasing the drug. By doing this, a highly optimized drug administration can be obtained.

Supplementary data to this article can be found online at https://doi.org/10.1016/j.matdes.2020.109212.

Data availability

All data is available in the main text or in the supplementary materials. Further details can be obtained from the authors upon reasonable request.

Author credit statement

Roberto Bernasconi metallized the devices, performed the actuation tests and wrote the manuscript; Emanuele Mauri coated with hydrogels the samples and performed the release tests; Arianna Rossetti coated with hydrogels the samples and performed the release tests; Stefano Rimondo coated with hydrogels the samples and performed the release tests; Raffaella Suriano 3D printed the devices; Marinella Levi supervised and wrote the manuscript; Alessandro Sacchetti supervised and wrote the manuscript; Salvador Pané supervised and wrote the manuscript; Luca Magagnin supervised and wrote the manuscript; Filippo Rossi supervised and wrote the manuscript.

Declaration of Competing Interest

The authors declare no conflict of interest.

References

[1] V. Venkateswarlu, Biopharmaceutics and Pharmacokinetics, PharmaMed Press, 2008.
[2] L. Shargel, B.C. Andrew, S. Wu-Pong, Applied Biopharmaceutics & Pharmacokinetics, Appleton & Lange Stamford 1999.
[3] B. Wang, L. Hu, T.J. Siahaan, Drug Delivery: Principles and Applications, John Wiley & Sons, 2016.
[4] M. Rowland, Influence of route of administration on drug availability, J. Pharm. Sci. 61 (1972) 70–74.
[5] O.C. Farokhzad, R. Langer, Nanomedicine: developing smarter therapeutic and diagnostic modalities, Adv. Drug Deliv. Rev. 58 (2006) 1456–1459.
[6] S.P. Vyas, R.K. Khar, Targeted & Controlled Drug Delivery: Novel Carrier Systems, CBS publishers & distributors, 2004.
[7] M.W. Tibbitt, J.E. Dahlman, R. Langer, Emerging frontiers in drug delivery, J. Am. Chem. Soc. 138 (2016) 704–717.
[8] M.W. Tibbitt, C.B. Rodell, J.A. Burdick, K.S. Anseth, Progress in material design for biomedical applications, Proc. Natl. Acad. Sci. 112 (2015) 14444–14451.
[9] G.A. Hughes, Nanostructure-mediated drug delivery, in: Nanomedicine in Cancer, Pan Stanford, 2017 47–72.
[10] T.M. Allen, P.R. Cullis, Liposomal drug delivery systems: from concept to clinical applications, Adv. Drug Deliv. Rev. 65 (2013) 36–48.
[11] B.S. Pattni, V.V. Chupin, V.P. Torchilin, New developments in liposomal drug delivery, Chem. Rev. 115 (2015) 10938–10966.
[12] Z. Ahmad, A. Shah, M. Siddiq, H.-B. Kraatz, Polymeric micelles as drug delivery vehicles, RSC Adv. 4 (2014) 17028–17038.
[13] R.H. Muller, C.M. Keck, Challenges and solutions for the delivery of biotech drugs–a review of drug nanocrystal technology and lipid nanoparticles, J. Biotechnol. 113 (2004) 151–170.
[14] J. Li, Z. Ding, Y. Li, J. Miao, W. Wang, K. Nundlall, S. Chen, Reactive oxygen species-sensitive thioketal-linked mesoporous silica nanoparticles as drug carrier for effective antibacterial activity, Mater. Des. 195 (2020) 109021.
[15] J. Ghitman, E.I. Biru, R. Stan, H. Iovu, Review of hybrid PLGA nanoparticles: future of smart drug delivery and theranostics medicine, Mater. Des. 193 (2020) 108805.
[16] S. Kakar, D. Batra, R. Singh, U. Nautiyal, Magnetic microspheres as magical novel drug delivery system: a review, J. Acute Dis. 2 (2013) 1–12, https://doi.org/10.1016/S2221-6189(13)60087-6.
[17] Q. Hu, H. Li, L. Wang, H. Gu, C. Fan, DNA nanotechnology-enabled drug delivery systems, Chem. Rev. 119 (2018) 6459–6506.
[18] S.W. Kim, R.V. Petersen, J. Feijen, Polymeric drug delivery systems, Drug Des. 10 (2016) 193–250.
[19] S. Karki, H. Kim, S.-J. Na, D. Shin, K. Jo, J. Lee, Thin films as an emerging platform for drug delivery, Asian J. Pharm. Sci. 11 (2016) 559–574.
[20] Y. Wang, L. Sun, Z. Mei, F. Zhang, M. He, C. Fletcher, F. Wang, J. Yang, D. Bi, Y. Jiang, 3D printed biodegradable implants as an individualized drug delivery system for local chemotherapy of osteosarcoma, Mater. Des. 186 (2020) 108336.
[21] S. Shah, M. Firlak, S. Berrow, N. Halcovitch, S. Baldock, B. Yousafzai, R. Hathout, J. Hardy, Electrochemically Enhanced Drug Delivery Using Polypyrrole Films, Materials (Basel) 11 (2018) 1123.
[22] S. Jiang, Y. Sun, X. Cui, X. Huang, Y. He, S. Ji, W. Shi, D. Ge, Enhanced drug loading capacity of polypyrrole nanowire network for controlled drug release, Synth. Met. 163 (2013) 19–23.
[23] T.R. Hoare, D.S. Kohane, Hydrogels in drug delivery: Progress and challenges, Polymer (Guildf). 49 (2008) 1993–2007.
[24] A.S. Hoffman, Hydrogels for biomedical applications, Adv. Drug Deliv. Rev. 64 (2012) 18–23.
[25] J. Li, D.J. Mooney, Designing hydrogels for controlled drug delivery, Nat. Rev. Mater. 1 (2016) 16071.
[26] W. Wei, Q. Zhang, W. Zhou, Z. Liu, Y. Wang, E.V. Alakpa, H. Ouyang, H. Liu, Immunomodulatory application of engineered hydrogels in regenerative medicine, Appl. Mater. Today 14 (2019) 126–136.
[27] T.K. Giri, A. Thakur, A. Alexander, H. Badwaik, D.K. Tripathi, Modified chitosan hydrogels as drug delivery and tissue engineering systems: present status and applications, Acta Pharm. Sin. B 2 (2012) 439–449.
[28] L. Agüero, D. Zaldivar-Silva, L. Pena, M.L. Dias, Alginate microparticles as oral colon drug delivery device: a review, Carbohydr. Polym. 168 (2017) 32–43.
[29] A. Chilkoti, M.R. Dreher, D.E. Meyer, D. Raucher, Targeted drug delivery by thermally responsive polymers, Adv. Drug Deliv. Rev. 54 (2002) 613–630.
[30] E. Mauri, F. Rossi, A. Sacchetti, Tunable drug delivery using chemoselective functionalization of hydrogels, Mater. Sci. Eng. C 61 (2016) 851–857.
[31] P. Gupta, K. Vermani, S. Garg, Hydrogels: from controlled release to pH-responsive drug delivery, Drug Discov. Today 7 (2002) 569–579.
[32] G.R. Mahdavinia, H. Etemadi, F. Soleymani, Magnetic/pH-responsive beads based on caboxymethyl chitosan and κ-carrageenan and controlled drug release, Carbohydr. Polym. 128 (2015) 112–121.
[33] X. Luo, X.T. Cui, Sponge-like nanostructured conducting polymers for electrically controlled drug release, Electrochem. Commun. 11 (2009) 1956–1959.
[34] J. Qu, X. Zhao, P.X. Ma, B. Guo, Injectable antibacterial conductive hydrogels with dual response to an electric field and pH for localized "smart" drug release, Acta Biomater. 72 (2018) 55–69.
[35] C. García-Astrain, L. Avérous, Synthesis and evaluation of functional alginate hydrogels based on click chemistry for drug delivery applications, Carbohydr. Polym. 190 (2018) 271–280.
[36] E. Mauri, S. Papa, M. Masi, P. Veglianese, F. Rossi, Novel functionalization strategies to improve drug delivery from polymers, Expert Opin. Drug Deliv. 14 (2017) 1305–1313.
[37] K.E. Peyer, L. Zhang, B.J. Nelson, Bio-inspired magnetic swimming microrobots for biomedical applications, Nanoscale. 5 (2013) 1259–1272.
[38] B.J. Nelson, L. Dong, F. Arai, Micro/nanorobots, Springer Handb. Robot. (2008) 411–450.
[39] J.J. Abbott, Z. Nagy, F. Beyeler, B.J. Nelson, Robotics in the small, part I: microbotics, IEEE Robot. Autom. Mag. 14 (2007) 92–103.
[40] X.-Z. Chen, M. Hoop, F. Mushtaq, E. Siringil, C. Hu, B.J. Nelson, S. Pané, Recent developments in magnetically driven micro-and nanorobots, Appl. Mater. Today 9 (2017) 37–48.
[41] D. Kagan, R. Laocharoensuk, M. Zimmerman, C. Clawson, S. Balasubramanian, D. Kang, D. Bishop, S. Sattayasamitsathit, L. Zhang, J. Wang, Rapid delivery of drug carriers propelled and navigated by catalytic nanoshuttles, Small. 6 (2010) 2741–2747, https://doi.org/10.1002/smll.201001257.
[42] F. Cheng, R. Yin, Y. Zhang, C.-C. Yen, Y. Yu, Fully plastic microrobots which manipulate objects using only visible light, Soft Matter 6 (2010) 3447–3449, https://doi.org/10.1039/c0sm00012d.
[43] D. Ahmed, T. Baasch, B. Jang, S. Pane, J. Dual, B.J. Nelson, Artificial swimmers propelled by acoustically activated flagella, Nano Lett. 16 (2016) 4968–4974.
[44] T. Xu, J. Yu, X. Yan, H. Choi, L. Zhang, Magnetic actuation based motion control for microrobots: an overview, Micromachines. 6 (2015) 1346–1364.
[45] D. Sun, S. Chen, D. Li, C. Liu, X. Li, S. Cheng, T. Luo, J. Yue, R. Wang, J. Li, Development of a magnetic microrobot for carrying and delivering targeted cells, Sci. Robot. 3 (2018)https://doi.org/10.1126/scirobotics.aat8829 eaat8829.
[46] F. Ullrich, S. Fusco, G. Chatzipirpiridis, S. Pané, B.J. Nelson, Recent progress in magnetically actuated microrobotics for ophthalmic therapies, Eur. Ophthalmic Rev. 8 (2014) 120–126.
[47] R. Bernasconi, E. Carrara, M. Hoop, F. Mushtaq, X. Chen, B.J. Nelson, S. Pané, C. Credi, M. Levi, L. Magagnin, Magnetically navigable 3D printed multifunctional microdevices for environmental applications, Addit. Manuf. 28 (2019) 127–135.
[48] D. Jang, J. Jeong, H. Song, S.K. Chung, Targeted drug delivery technology using untethered microrobots: a review, J. Micromech. Microeng. 29 (2019) 53002.
[49] S. Fusco, H.-W. Huang, K.E. Peyer, C. Peters, M. Häberli, A. Ulbers, A. Spyrogianni, E. Pellicer, J. Sort, S.E. Pratsinis, Shape-switching microrobots for medical applications: the influence of shape in drug delivery and locomotion, ACS Appl. Mater. Interfaces 7 (2015) 6803–6811.
[50] S. Lee, S. Kim, S. Kim, J. Kim, C. Moon, B.J. Nelson, H. Choi, A capsule-type microrobot with pick-and-drop motion for targeted drug and cell delivery, Adv. Healthc. Mater. 7 (2018) 1700985.
[51] H. Li, G. Go, S.Y. Ko, J.-O. Park, S. Park, Magnetic actuated pH-responsive hydrogel-based soft micro-robot for targeted drug delivery, Smart Mater. Struct. 25 (2016) 27001.
[52] C. Peters, M. Hoop, S. Pané, B.J. Nelson, C. Hierold, Degradable magnetic composites for minimally invasive interventions: device fabrication, targeted drug delivery, and cytotoxicity tests, Adv. Mater. 28 (2016) 533–538.
[53] R. Bernasconi, F. Cuneo, E. Carrara, G. Chatzipirpiridis, M. Hoop, X. Chen, B.J. Nelson, S. Pané, C. Credi, M. Levi, L. Magagnin, Hard-magnetic cell microscaffolds from electroless coated 3D printed architectures, Mater. Horizons. 5 (2018) 699–707, https://doi.org/10.1039/C8MH00206A.
[54] R. Bernasconi, C. Credi, M. Tironi, M. Levi, L. Magagnin, Electroless metallization of Stereolithographic Photocurable resins for 3D printing of functional microdevices, J. Electrochem. Soc. 164 (2017) B3059–B3066, https://doi.org/10.1149/2.0081705jes.
[55] E. Mauri, P. Veglianese, S. Papa, A. Mariani, M. De Paola, R. Rigamonti, G.M.F. Chincarini, I. Vismara, S. Rimondo, A. Sacchetti, Double conjugated nanogels for selective intracellular drug delivery, RSC Adv. 7 (2017) 30345–30356.
[56] S. Mandal, A. Sahana, A. Banerjee, D.A. Safin, M.G. Babashkina, K. Robeyns, S. Verkaart, J.G.J. Hoenderop, M.P. Mitoraj, Y. Garcia, A smart rhodamine–pyridine conjugate for bioimaging of thiocyanate in living cells, RSC Adv. 5 (2015) 103350–103357.
[57] T. Taweetanavanich, B. Wanno, T. Tuntulani, B. Pulpoka, C. Kaewtong, A pH optical and fluorescent sensor based on rhodamine modified on activated cellulose paper, J. Chin. Chem. Soc. 66 (2019) 493–499.
[58] M. Bio, P. Rajaputra, Y. You, Photodynamic therapy via FRET following bioorthogonal click reaction in cancer cells, Bioorg. Med. Chem. Lett. 26 (2016) 145–148.
[59] M.P. Kummer, J.J. Abbott, B.E. Kratochvil, R. Borer, A. Sengul, B.J. Nelson, Octomag: an electromagnetic system for 5-DOF wireless micromanipulation, IEEE Trans. Robot. 26 (2010) 1006–1017, https://doi.org/10.1109/TRO.2010.2073030.
[60] C.M. Comisar, S.E. Hunter, A. Walton, P.E. Savage, Effect of pH on ether, ester, and carbonate hydrolysis in high-temperature water, Ind. Eng. Chem. Res. 47 (2008) 577–584.

[61] F.H. Chen, Q. Gao, J.Z. Ni, The grafting and release behavior of doxorubincin from Fe3O4@ SiO2 core–shell structure nanoparticles via an acid cleaving amide bond: the potential for magnetic targeting drug delivery, Nanotechnology. 19 (2008) 165103.

[62] L. Liang, D. Astruc, The copper (I)-catalyzed alkyne-azide cycloaddition (CuAAC)"click" reaction and its applications. An overview, Coord. Chem. Rev. 255 (2011) 2933–2945.

[63] Y.L. Li, W.X. Wang, Y. Wang, W.B. Zhang, H.M. Gong, M.X. Liu, Synthesis and Characterization of Rhodamine B-Ethylenediamine-Hyaluronan Acid as Potential Biological Functional Materials, in: IOP Conf, IOP Publishing, Ser. Mater. Sci. Eng, 2018 12040.

[64] J.W. Jeong, B.A. Rao, J.-Y. Lee, J.-Y. Hwang, Y.-A. Son, An 'OFF–ON'fluorescent chemosensor based on rhodamine 6G-2-chloronicotinaldehyde for the detection of Al3+ ions: part II, Sensors Actuators B Chem. 227 (2016) 227–241.

[65] P.L. Ritger, N.A. Peppas, A simple equation for description of solute release II. Fickian and anomalous release from swellable devices, J. Control. Release 5 (1987) 37–42.